https://doi.org/10.3311/PPch.37752

Periodica Polytechnica Chemical Engineering, 68(4), pp. 587–596, 2024

Kinetic and Chemical Analysis of Pyrolysis in *Bambusa vulgaris* Leaves and Derived Fibers

Prabhuteja Pokuri[1], Vijetha Ponnam[1*], Venkata Kishore Babu Ponnam[2], Solomon Godwin Babu Neelamegam David[1], Subbaiah Tondepu[1]

[1] Department of Chemical Engineering, VFSTR (Deemed to be) University, Vadlamudi, 522213 Guntur, Andhra Pradesh, India
[2] Department of Electrical and Electronics Engineering, R.V.R. & J.C. College of Engineering, Chowdavaram, 522006 Guntur, Andhra Pradesh, India
* Corresponding author, e-mail: vijetha.ponnam@gmail.com

Received: 22 June 2024, Accepted: 25 October 2024, Published online: 22 November 2024

Abstract

Bamboo, a perennial and monocarpic plant, holds immense potential beyond its commonly recognized applications. In this study, fiber was extracted from bamboo leaves. Pyrolytic kinetic studies were done on leaves and the extracted fibers, utilizing thermogravimetry and derivative thermogravimetry (TG/DTG) data obtained at heating rates 10, 20, and 30 K/min within the temperature range of 298–1093 K. Model-free methods such as Ozawa-Flynn-Wall (OFW), Kissinger-Akahira-Sunose (KAS), and Friedman were employed to calculate the activation energy (E_a) and the pre-exponential factor (A). For leaves, the calculated E_a values were found to be 283 kJ/mol (KAS), 279 kJ/mol (OFW), and 318 kJ/mol (Friedman), while the A values were determined as 7.2×10^{43} s^{-1} (KAS), 1.07×10^{43} s^{-1} (OFW), and 5.7×10^{45} s^{-1} (Friedman). In the case of fiber, the E_a values were found to be 162 kJ/mol (KAS), 164 kJ/mol (OFW), and 165 kJ/mol (Friedman), with corresponding A of 4.6×10^{15} s^{-1} (KAS), 5.6×10^{13} s^{-1} (OFW), and 348×10^{13} s^{-1} (Friedman). Additionally, scanning electron microscope (SEM), energy dispersive X-ray spectroscopy (EDX), and Fourier transform infrared spectroscopy (FTIR) analyses were conducted on both leaves and fiber.

Keywords

Ozawa-Flynn-Wall (OFW), Kissinger-Akahira-Sunose (KAS), Friedman, scanning electron microscopy, pre-exponential factor, activation energy

1 Introduction

Biomass, derived from a variety of flora and fauna, serves as a carbon-rich material with numerous applications. Like fossil fuels, biomass has found its way into power generation, biofuel production, and more. Over the past decade, there has been a significant increase in the production of biochar from biomass. Biomass represents a diverse catalog of materials, including leaves, roots, and manure, which find utility in various fields, such as medicine, construction, and furniture. However, waste is inevitable in every sector, and the remnants of plants often end up in landfills. Incineration is a technique where materials are burned in the presence of oxygen, while pyrolysis occurs in the absence of oxygen [1]. Pyrolysis, in comparison to incineration, offers several advantages as it produces biochar instead of ash. Kinetic studies play a crucial role in understanding the reaction mechanisms of pyrolysis and gaining insights into forest fires [2].

Pyrolytic kinetic studies involve analyzing the reactions occurring during pyrolysis from two distinct perspectives: the scientific aspect and the technical aspect [3]. The scientific approach focuses on developing models to understand and interpret the individual steps of the pyrolysis process. Hypotheses are formulated and compared with experimental results, leading to further experiments that support or refine the initial hypotheses. On the other hand, the technical approach utilizes kinetic analysis as a tool for data reduction and prediction. The objective is to extract essential information from complex datasets and create simplified models with a few parameters for practical applications. Both approaches require the establishment of kinetic models and the specification of their parameters to achieve comprehensive solutions applicable to a wide range of test conditions. Although the scientific and technical perspectives have different goals, they

Cite this article as: Pokuri, P., Ponnam, V., Ponnam, V. K. B., Neelamegam David, S. G. B., Tondepu, S. "Kinetic and Chemical Analysis of Pyrolysis in *Bambusa vulgaris* Leaves and Derived Fibers", Periodica Polytechnica Chemical Engineering, 68(4), pp. 587–596, 2024. https://doi.org/10.3311/PPch.37752

share common steps that contribute to the overall understanding and optimization of pyrolysis processes and the results obtained from the kinetic studies would be helpful to design an efficient pyrolysis reactor [4, 5].

One area of interest within biomass research is bamboo, specifically the *Bambusa vulgaris* species. Bamboo belongs to the genus of large perennial, monocarpic grass and has found widespread use in numerous daily life applications. When people think of bamboo, the stem is often the first and most recognizable part that comes to mind. However, leaves are often categorized as waste and overlooked in many applications. While certain species of bamboo have some applications in medicine [6], there is a significant research gap in fully utilizing the potential of bamboo leaves. Modern researchers are exploring the use of bamboo leaf ash as filler materials in concrete and mortar [7]. Additionally, leaf biomass is being utilized for the adsorption of heavy metals and textile dyes [8, 9]. Interestingly, research suggests that a hectare of bamboo plantation sheds around 8 to 11 tons of leaves per year, which can be collected easily. These leaves have been utilized as a source for fiber extraction as fibers are also playing major role as filler materials in cement [10, 11] and in making polymer composites [12] etc. The obtained *B. vulgaris* fibers (BVF), along with *B. vulgaris* leaves (BV), were subjected to thermogravimetric analysis (TGA) for pyrolytic kinetic studies. The activation energy (E_a) and pre-exponential factors (A) with respect to conversion factors were calculated using the Kissinger-Akahira-Sunose (KAS), Ozawa-Flynn-Wall (OFW), and Friedman models.

2 Materials and methods

2.1 Materials and chemicals

Bamboo leaves were procured from local market and commercial grade chemicals were used for experimentation.

2.2 Method

2.2.1 Fiber extraction

The fiber extraction starts with the regular cleaning of the leaves to remove the dust and the unwanted matter from them. Then the leaves were soaked in 10% aqueous NaOH for overnight. The next day the soaked leaves were transferred into freshly prepared 10% NaOH solution with a gram:ml ratio of 1:10 (leaves: solution) and boiled for 2 h. After that, the fibers were filtered, and water washed and neutralized by adding 10% acetic acid. The extracted fibers were then made in to sheets as shown in Fig. 1. Physicochemical analysis was conducted for both the extracted fiber and *B. vulgaris*.

Fig. 1 *B. vulgaris* – derived fiber sheets

Using the data obtained by thermogravimetry and derivative thermogravimetry (TG/DTG), the pyrolytic kinetic studies were carried to find the E_a and the A.

2.3 TG/DTG analysis

TG/DTG is a technique used to study the thermal behavior of a sample by measuring its mass changes as a function of temperature. The TG/DTG analysis is performed on two samples: BV and BVF. The analysis is conducted using the Simultaneous Thermal Analyzer (STA 7200, Hitachi HTG, Japan) at three different heating rates 10, 20, and 30 K/min in nitrogen atmosphere with a flow rate of 30 mL/min. The temperature range for the analysis spans from 298 K (room temperature) to 1093 K.

2.4 FTIR analysis

Fourier transform infrared spectroscopy (FTIR) is a widely used technique in chemistry that provides information about the chemical composition of a sample by measuring its infrared absorption spectra. The FTIR analysis is performed using the Cary 630 FTIR spectrometer with a Diamond ATR (Attenuated Total Reflectance) accessory, manufactured by Agilent Technologies in the USA. By measuring the infrared spectra of the BV and BVF samples, the FTIR analysis can identify the functional groups present in the samples.

2.5 EDX analysis

Energy dispersive X-ray spectroscopy (EDX) analysis for BV, BVF was done by using EDX (EDAX Inc., USA) equipment. It would involve bombarding the samples with high-energy electrons or X-rays and detecting the characteristic X-rays emitted. By analyzing the energies of these X-rays, the elements present in BV and BVF can be identified, including those with atomic numbers higher than helium. The results obtained from EDX analysis provide information about the elemental composition of the samples.

2.6 SEM analysis

Scanning electron microscope (SEM) is used to observe the surface morphology of the samples at micrometer scale. SEM is also used to calculate the average grain size of the particles prior to TEM and particle size analysis. To observe the surface morphology of BV, BVF, biochar of BV and biochar of BVF (BVFBC), SEM (VEGA 3, SBH, TESCAN Brno S.R.O., Czech Republic) was used.

2.7 Kinetic studies

Generally, the basic assumption of the pyrolysis equation is:

$$\text{Biomass} \rightarrow \text{Biochar} + \text{Volatile Gases}.$$

The rate equation for this pyrolysis process is given by:

$$\frac{dC_f}{dt} = Kf\left(C_f\right), \tag{1}$$

where:

- K = rate constant;
- C_f = conversion factor and given by $C_f = (m_i - m_t)/(m_i - m_f)$;
- m_i = initial mass of biomass;
- m_t = instantaneous mass of sample;
- m_f = final mass of biochar;
- $f(C_f)$ = the function depends on mechanism, mentioned in Table 1.

When the pyrolysis reaction is assumed as a single step reaction, then K can be defined as:

$$K = A \times e^{-\frac{E_a}{R \times T}}, \tag{2}$$

where:

- A: pre-exponential factor (s^{-1});
- E_a: activation energy (KJ/mol);
- T: temperature (K).

By combining Eqs. (1) and (2) we get:

$$\frac{dC_f}{dt} = f\left(C_f\right) \times A \times e^{-\frac{E_a}{R \times T}}. \tag{3}$$

From the heating rate defined as $\beta = dT/dt$:

$$dt = \frac{dT}{\beta}. \tag{4}$$

where:

- d_t: change in time (s);
- d_T: change in temperature (K).

After substituting Eq. (4) in Eq. (3) and integrating on both sides, gives:

$$\int_0^{C_f} \frac{d\left(C_f\right)}{f\left(C_f\right)} = \int_0^T A \times \exp\left(\frac{-E_a}{R \times T}\right)\frac{dT}{\beta} = g\left(C_f\right). \tag{5}$$

In this work, to find E_a and A, mainly three iso-conversional model free methods were used, those are KAS, OFW and Freidman methods. Iso-conversional model free methods center around assessing the E_a using the conversion rate, which is dependent on temperature. Consequently, the reaction rate at a particular conversion level (C_f) for a given heating rate (β_i) solely relies on temperature (T), with $f(C_f)$ remaining constant.

2.7.1 Method 1: Kissinger-Akahira-Sunose (KAS) method

The E_a and A can be determined accurately by using KAS method. On doing some rearrangements to the Eq. (3), we get:

$$\ln\frac{\beta}{T^2} = \ln\frac{A \times R}{g\left(C_f\right) \times E_a} - \frac{E_a}{R \times T}. \tag{6}$$

The plot between $\ln(\beta/T^2)$ (Y-axis) vs. $1/T$ at individual conversion factor (C_f) for three different heating rates gives straight lines for all the conversions. The slope of each line represents $-E_a/R$ and the intercept gives the value of $\ln(A \times R/g(C_f) \times E_a)$.

2.7.2 Method 2: Ozawa-Flynn-Wall (OFW) method

The equation for this model is given by:

$$\log\left(\beta\right) = \log\left[\frac{A \times E_a}{-R \times g\left(C_f\right)}\right] - 2.315 - 0.457\frac{E_a}{R \times T}. \tag{7}$$

A plot between $\log \beta$ vs. $1/T$ at individual C_f for three different heating rates gives straight lines for all the conversions. The slope of each line represents $-0.457E_a/R$ and the intercept gives the value of $\log[(A \times E_a)/(-R \times g(C_f))] - 2.315$.

2.7.3 Method 3: Friedman method

Both OFW and KAS methods use integration technique, Friedman method uses differentiation technique to calculate E_a and A. The equation for this model is given by taking natural logarithm for the Eq. (3) gives:

$$\ln\frac{dC_f}{dt} = \ln\left(A \times f\left(C_f\right)\right) - \frac{E_a}{R \times T}. \tag{8}$$

A plot between $-E_a/R$ at individual C_f for different heating rates gives straight lines and the slope represents $1/T$ and the intercept represents $\ln(A \times f(C_f))$.

In these three equations, $f(C_f)$ and $g(C_f)$ represent various kinetic models representing the interaction between different phases, random formation of nuclei, growth of nuclei, chemical reactions, and diffusion are employed to analyze the data obtained from TGA. In this study, the TGA data collected during the pyrolysis of BV and BVF were examined using 14 different kinetic models, as presented in Table 1. The most appropriate reaction model is determined based on the highest regression coefficient observed in the plot of $\ln[g(C_f)/T^2]$ vs. $1/T$.

3 Results and discussions

3.1 TG/DTG

The thermal stability of BV and BVF was investigated through TG/DTG analysis, as shown in Fig. 2 (a) and (b). The analysis was conducted at heating rates of 10, 20, and 30 K/min, with sample sizes for BV being 3.4 mg, 3.5 mg, and 3.7 mg, and for BVF, 3.3 mg, 3.2 mg, and 3.7 mg for the respective heating rates. The TG/DTG results were further utilized for kinetic studies.

For BV, the major mass loss was observed between 473 and 693 K, while BVF exhibited mass loss from 523 to 723 K with similar DTG curves. The initial peak, ranging from 313–393 K, corresponded to the evaporation of moisture and volatile matter, accounting for approximately 10% mass loss in BV and 8% in BVF. The second, major mass loss stage was attributed to the decomposition of hemicellulose, lignin, and cellulose, which extended up to 723 K for BVF.

When comparing the thermal decomposition rates, BV demonstrated a lower mass loss rate (763.5 µg/min at 30 K/min) than BVF (1018.2 µg/min at 30 K/min) around the same peak temperature, approximately 623 K. This suggests that BV is thermally more stable than BVF. The TG analysis further supported this, showing that BVF

Table 1 Solid state kinetic models

Model	Mechanism name	$f(C_f)$	$g(C_f)$
		Chemical reaction	
1	First order	$(1-C_f)$	$[-\ln(1-C_f)]$
2	Second order	$(1-C_f)^2$	$(1-C_f)^{-1}-1$
3	Third order	$(1-C_f)^3$	$[(1-C_f)^{-2}-1]/2$
4	Nth order	$(1-C_f)^n$	$[(1-C_f)^{1-n}-1]/(n-1)$
		Random nucleation and nuclei growth	
5	Two-dimensional	$2(1-C_f)[-\ln(1-C_f)]^{\frac{1}{2}}$	$[-\ln(1-C_f)]^{\frac{1}{2}}$
6	Three-dimensional	$3(1-C_f)[-\ln(1-C_f)]^{\frac{2}{3}}$	$[-\ln(1-C_f)]^{\frac{1}{3}}$
		Limiting surface reaction between both phases	
7	One dimension	1	C_f
8	Two dimensions	$2(1-C_f)^{\frac{1}{2}}$	$1-(1-C_f)^{\frac{1}{2}}$
9	Three dimensions	$3(1-C_f)^{\frac{1}{2}}$	$1-(1-C_f)^{\frac{1}{3}}$
		Diffusion	
10	One way transport	$\frac{1}{2}C_f$	C_f^2
11	Two way transport	$[-\ln(1-C_f)]^{-1}$	$C_f+(1-C_f)\ln(1-C_f)$
12	Three way transport	$\frac{2}{3}(1-C_f)^{\frac{2}{3}}/[1-(1-C_f)^{\frac{1}{3}}]$	$[1-(1-C_f)^{\frac{1}{3}}]^2$
13	Ginstling-Brounshtein equation	$\frac{2}{3}(1-C_f)^{\frac{1}{3}}/[1-(1-C_f)^{\frac{1}{3}}]$	$(1-2C_f)/(3-(1-C_f))^{\frac{2}{3}}$
14	Zhuravlev equation	$\frac{2}{3}(1-C_f)^{\frac{5}{3}}/[1-(1-C_f)^{\frac{1}{3}}]$	$[-\frac{1}{3}(1-C_f)-1]^2$

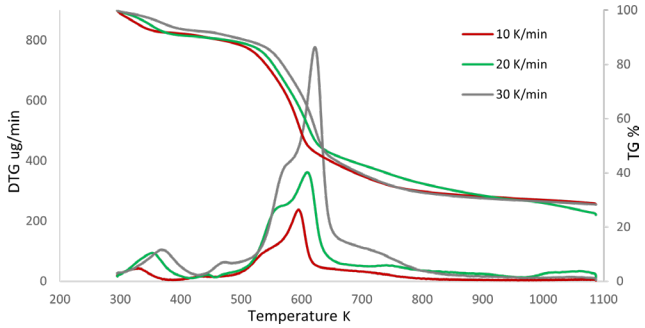

(a)

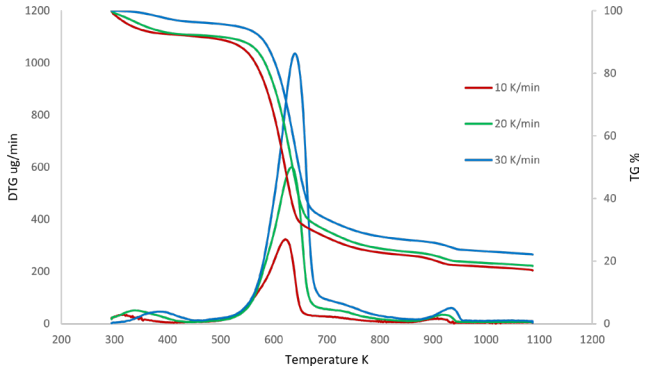

(b)

Fig. 2 TG/DTG of (a) BV; (b) BVF

had a total mass loss of around 80%, whereas BV had a mass loss of around 70% from room temperature to 1093 K. This difference could be attributed to the partial decomposition of lignin during the fiber extraction process.

A significant observation in both TG/DTG curves is the shift of the maximum decomposition temperature (T_{max}) to higher temperatures with increasing heating rates. The T_{max} for BV was observed at 591 K, 633 K, and 643 K at heating rates of 10, 20, and 30 K/min, respectively. This shift, along with the corresponding increase in the rate of mass loss, is indicative of a heat transfer limitation, likely caused by thermal lag within the materials [13, 14]. As the heating rate increases, the temperature rises more rapidly, leading to a faster reaction rate and greater mass loss compared to lower heating rates.

3.2 FTIR analysis

The FTIR for BV, BVF, BVFBC is depicted in Fig. 3 within a range of 4000–500 cm^{-1}. The peaks in the region 1000–500 cm^{-1} corresponding to the presence of functional groups Si-O and Al-OH were observed. The wider peak at 3332 cm^{-1} indicates the stretching vibration of O-H group in polysaccharides, which is vanished in BVFBC, due to the pyrolysis. The peaks in range of 3660–2900 cm^{-1} indicate the O-H and C-H bonds in polysaccharides in BV

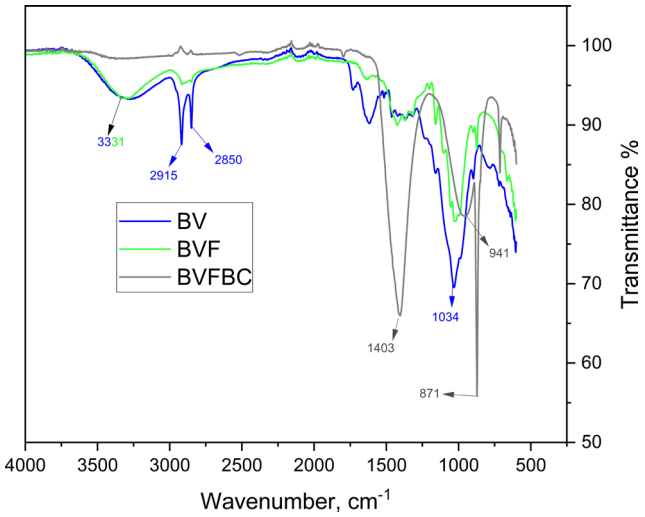

Fig. 3 FTIR analysis

and BVF [8]. BVFBC has the least peaks due to pyrolysis and the peak in BVFBC at 871 cm^{-1} corresponding to the Si-CH_3 vibration and indicates the presence of Si. The peaks at 918 cm^{-1} in BL correspond to the vibration of N-H and -OH bonds. A fraction of those evaporated/decomposed during the process of extraction, leading to lower peak intensity in BVF and completely decomposed during the pyrolysis stage.

3.3 EDX analysis

Fig. 4 (a) and (b) indicates the EDX of BV and BVF respectively. This indicates the presence of elements Si, K, C and O in the leaves and only C and O with a small trace of Si is present in the fibers, the elements like K and Si may be leached away during the extraction process with NaOH.

3.4 SEM analysis

Fig. 5 (a), (b), (c) and (d) represents BV, BVF, biochar of BV and BVFBC respectively. The surface of the leaf is roughly packed and there is no trace of fiber like structures due to the existence of lignin. After the extraction process the fibers are clearly visible with a diameter ranging from 4.2–4.6 µm.

When compared to BVFBC, biochar of BV has more widened pores. These types of pores will increase the surface area which will be helpful in some process like adsorption, where as the formed BVFBC particles have less pores than BV biochar.

3.5 Kinetics studies

The pyrolytic kinetic studies of BV and BVF were carried out with the C_f ranging from 0.2–0.9. For the accurate

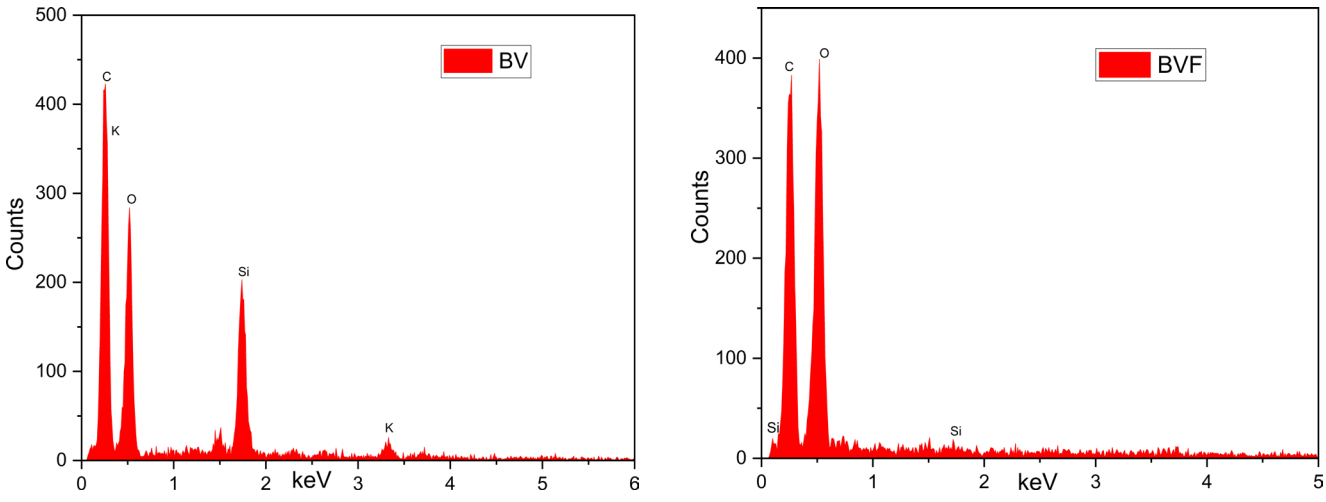

(a) (b)

Fig. 4 EDX of (a) BV; (b) BVF

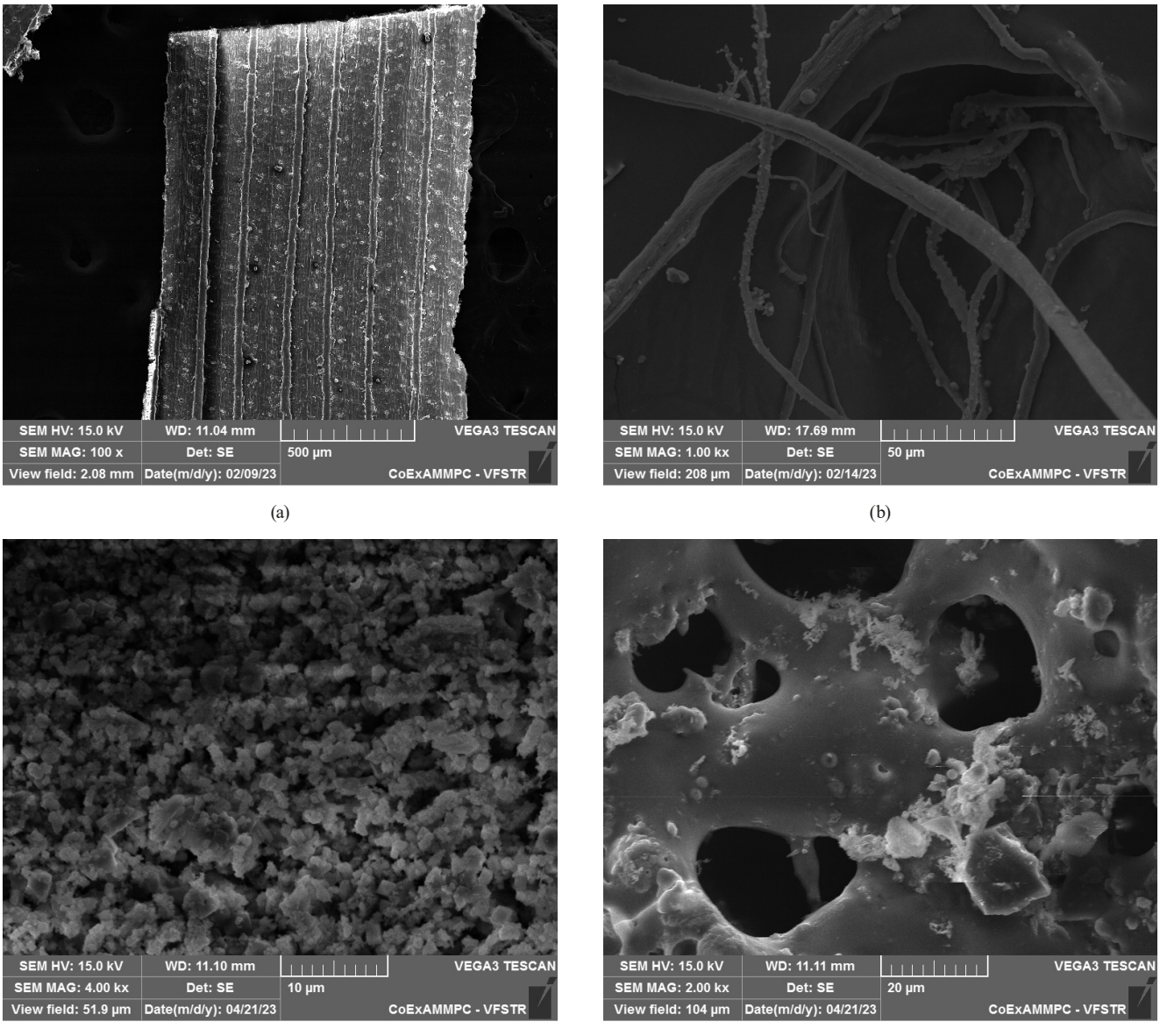

(a) (b)

(c) (d)

Fig. 5 SEM image of (a) BV; (b) BVF; (c) BVF biochar; (d) BV biochar

Table 2 R^2 values of 13 solid state kinetic equations

Model	Mechanism name	R^2 values					
		10 K/min		20 K/min		30 K/min	
		BV	BVF	BV	BVF	BV	BVF
		Chemical reaction					
1	First order	0.8375	0.8149	0.4119	0.8304	0.8851	0.8955
2	Second order	0.8729	0.8187	0.9108	0.8150	0.8798	0.8975
3	Third order	0.8175	0.7680	0.8063	0.7540	0.8078	0.8314
		Random nucleation and nuclei growth					
4	Two-dimensional	0.0639	0.2231	0.2744	0.2871	0.2810	0.6883
5	Three-dimensional	0.6176	0.4843	0.3521	0.4392	0.4958	0.0477
		Limiting surface reaction between both phases					
6	One dimension	0.4194	0.5562	0.8216	0.6057	0.5761	0.7790
7	Two dimensions	0.6560	0.7050	0.7071	0.7319	0.7485	0.8348
8	Three dimensions	0.7290	0.7497	0.7636	0.7722	0.8035	0.8571
		Diffusion					
9	One way transport	0.7756	0.8082	0.786	0.8222	0.8254	0.8683
10	Two way transport	0.8274	0.8364	0.8323	0.8486	0.8656	0.8874
11	Three way transport	0.8837	0.8689	0.8117	0.8789	0.9116	0.9123
12	Ginstling-Brounshtein equation	0.8489	0.8489	0.8523	0.8602	0.8829	0.8963
13	Zhuravlev equation	0.9273	0.8875	0.9417	0.8924	0.9435	0.9380

measurement of the E_a and A, the moisture evaporation zone isn't advisable to consider into the account while doing calculations. The R^2 values at three different heating rates for both BV and BVF for the plot $\ln[g(C_f)/T^2]$ vs. $1/T$ are tabulated in Table 2.

Zhuravlev's diffusion equation is found to be best fit for both materials at all three heating rates. So, $[(1 - C_f) \times ((-1)/3) - 1]^2$ was considered as $g(C_f)$ and $(2/3) \times (1 - C_f)^{5/3} / [1 - (1 - C_f)^{1/3}]$ was considered as $f(C_f)$ for solving KAS, OFW and Friedman equations.

3.5.1 Activation energy

E_a and the A values for BV and BVF were calculated by using OFW, KAS and Friedman methods and are shown in Fig. 6 (a), (b) and (c). The E_a values for different C_f along with the R^2 values were tabulated. The E_a is increasing as the C_f increases. This is due to the increase of the complexation of the reactions happening in the samples.

3.5.2 Pre-exponential factor

A gives the idea of number of collisions per unit time. Like E_a, A also increases with temperature. As the reaction rate increases, the number of collisions increases.

The E_a for the leaves (BV) (calculated from graphs, shown in Fig. 6 (a), (b) and (c) and tabulated in Table (3)) is higher when compared to the BVF (Table 4), because of the leaf contains a greater number of compounds mostly lost during the process of extraction. The activation energies for BV are 283.8, 279.8 and 318.9 kJ/mol. The activation energies range from 170–670 kJ/mol and the highest activation is at C_f 0.9 for Friedman method. The A is ranging from the order of 10^{15} to 10^{45} s^{-1} and the average value is 10^{43} s^{-1}. The drastic increase of A from power 15 to power 45 in C_f 0.7, 0.8 and 0.9 is due to the temperature rise, leading to more collisions among the molecules. This trend is observed in three models.

For BVF see the results in Fig. 7.

From the graphs Fig. 7 (a), (b) and (c), E_a values and A were calculated and tabulated in Table 4 for BVF and the calculated E_a is in range of 100–195 kJ/mol. The average E_a for BVF were 162.4, 164.4 and 165.5 kJ/mol for KAS, OFW and Friedman methods, respectively. The Friedman method showed more deviation at individual C_f values when compared to OFW and KAS, but the average E_a is nearly equal to that from OFW and KAS. These results were well aligned with the previous findings for plant residue pyrolysis [15–17].

For BVF the number of collisions increased from order 10^6 to order 10^{16} as the temperature increased. The number of collisions is very low compared to BV. The reason

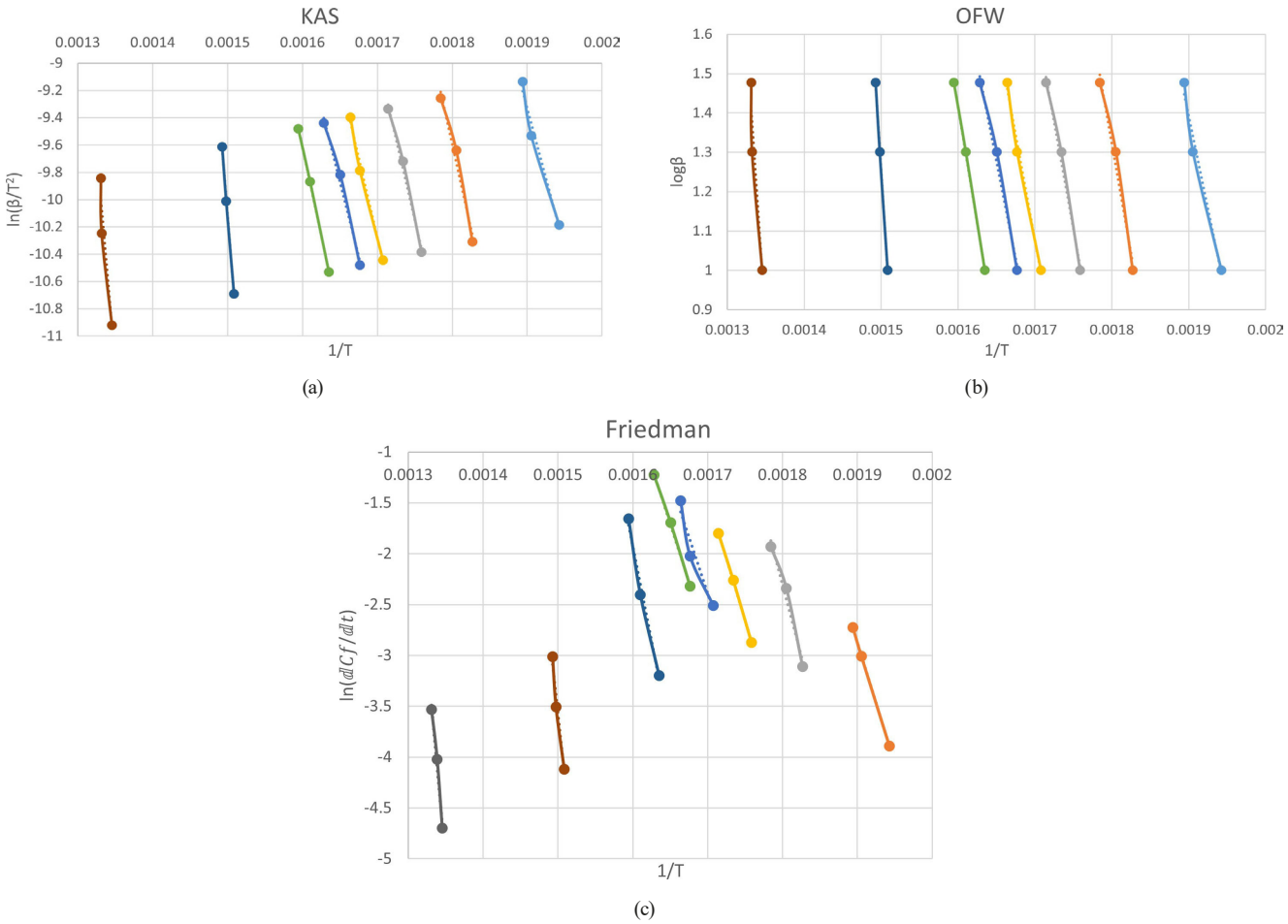

Fig. 6 BV graph for (a) KAS model (b) OFW model (c) Friedman model

Table 3 E_a and A values from 3 models for BV

	KAS			OFW			Friedman		
C_f	E_a (kJ/mol)	A (s^{-1})	R^2 values	E_a (kJ/mol)	A (s^{-1})	R^2 values	E_a (kJ/mol)	A (s^{-1})	R^2 values
0.2	171.50	1.15×10^{15}	0.9764	171.21	1.12×10^{15}	0.9786	199.21	5.21×10^{17}	0.9999
0.3	205.03	5.21×10^{17}	0.9790	203.61	4.04×10^{17}	0.9808	230.53	1.43×10^{20}	0.9737
0.4	198.11	5.05×10^{16}	0.9912	198.13	4.49×10^{16}	0.9920	202.58	1.28×10^{17}	0.9995
0.5	194.11	9.62×10^{15}	0.992	193.84	9.48×10^{15}	0.9927	182.89	1.58×10^{15}	0.9287
0.6	181.66	6.52×10^{4}	0.9883	182.18	7.61×10^{14}	0.9895	190.56	8.77×10^{15}	0.9988
0.7	215.89	4.6×10^{17}	0.9996	214.94	4.07×10^{17}	0.9997	311.49	5.82×10^{25}	0.9866
0.8	569.88	5.77×10^{44}	0.9990	552.08	8.58×10^{43}	0.9990	563.96	3.92×10^{43}	0.9688
0.9	533.67	3.92×10^{37}	0.9012	518.96	8.34×10^{36}	0.9053	670.28	4.57×10^{46}	0.9836
Average	283.835	7.21×10^{43}	0.9783	279.37	1.07×10^{43}	0.9797	318.940	5.72×10^{45}	0.9799

Table 4 E_a and A values from 3 models for BVF

	KAS			OFW			Friedman		
C_f	E_a (kJ/mol)	A	R^2	E_a (kJ/mol)	A	R^2	E_a (kJ/mol)	A	R^2
0.2	102.0128	7.00×10^{6}	0.8813	106.0899	2.27×10^{7}	0.8992	150.2007	4.96×10^{11}	0.953
0.3	133.9552	7.14×10^{9}	0.9204	136.7425	1.46×10^{10}	0.9304	180.9376	2.71×10^{14}	0.9626
0.4	163.1124	3.06×10^{12}	0.9366	164.6663	4.49×10^{12}	0.9435	203.5267	2.5×10^{16}	0.9666
0.5	175.8744	4.33×10^{13}	0.9360	176.9553	5.67×10^{13}	0.9426	36.39537	210.3944	0.0214
0.6	174.2282	3.55×10^{13}	0.9405	175.5436	4.88×10^{13}	0.9468	188.2705	1.54×10^{15}	0.9633
0.7	181.0706	1.46×10^{14}	0.9537	182.1984	1.91×10^{14}	0.9586	181.5112	4.38×10^{14}	0.9708
0.8	178.5515	8.10×10^{13}	0.9730	180.0299	1.14×10^{14}	0.976	187.5971	6.24×10^{14}	0.9899
0.9	190.6982	2.44×10^{13}	0.9353	193.0048	3.88×10^{13}	0.9427	195.6284	2.72×10^{13}	0.8644
Average	162.4378	4.16×10^{13}	0.9346	164.4038	5.68×10^{13}	0.9424	165.5085	3.49×10^{15}	0.8365

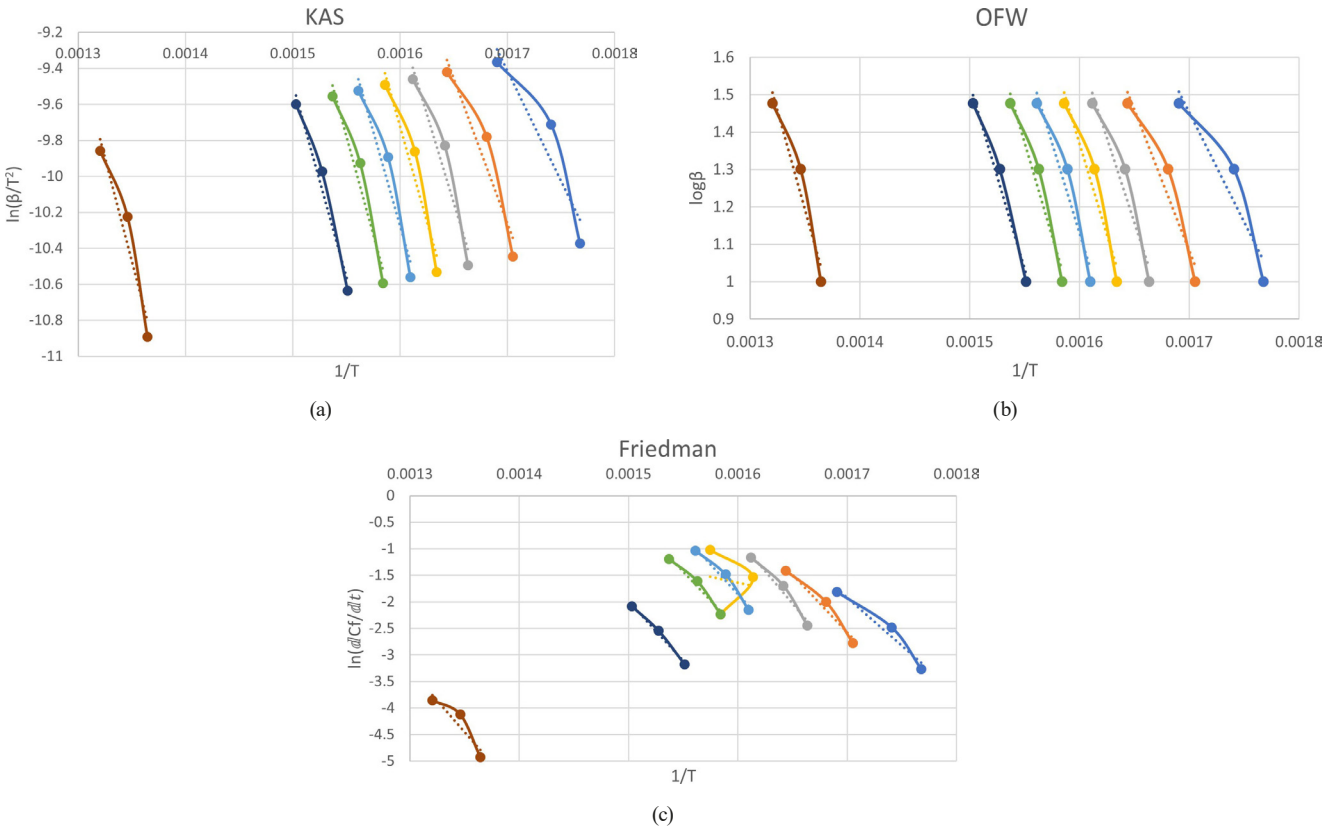

Fig. 7 BVF graphs for; (a) KAS model; (b) OFW model; (c) Friedman model

behind this is the same as the reason for lower E_a of BVF compared to BV. The highest number of collisions is evaluated to be 2.5×10^{15}.

4 Conclusions

The aim of this paper is to utilize the BV to extract fibers and to conduct pyrolytic kinetic studies for both leaves and fibers. Along with that, physicochemical characterisation methods like SEM, FTIR, EDX and TG/DTG were applied. TG showed that the maximum temperature that the leaves can resist is up to 473 K, from which the actual decomposition of the material started and for the fibers it is 493 K. EDX showed that Si concentration was decreased in the process of extracting fibers and SEM showed the clear morphology of the fibers and the leaves.

When the results of both BV and BVF are compared, the average E_a of the fiber (165 kJ/mol) is smaller than the leaves (293 kJ/mol). The same repeats with the A also. This is due to the complexity of the reactions happening in the leaves and most of the compounds in the leaves were disintegrated/leached during the extraction. Due to this, it took 43% less energy to kick starts the reaction process for the fibers compared to leaves. Due to the complex molecules, the A in leaves rose to the 10^{45} s^{-1} at $C_f = 0.8$.

References

[1] Miller, R. S., Bellan, J. "A Generalized Biomass Pyrolysis Model Based on Superimposed Cellulose, Hemicelluloseand Liqnin Kinetics", Combustion Science and Technology, 126(1–6), pp. 97–137, 1997. https://doi.org/10.1080/00102209708935670

[2] Yao, F., Wu, Q., Lei, Y., Guo, W., Xu, Y. "Thermal decomposition kinetics of natural fibers: Activation energy with dynamic thermogravimetric analysis", Polymer Degradation and Stability, 93(1), pp. 90–98, 2008. https://doi.org/10.1016/j.polymdegradstab.2007.10.012

[3] Opfermann, J. "Kinetic Analysis Using Multivariate Non-linear Regression. I. Basic concepts", Journal of Thermal Analysis and Calorimetry, 60(2), pp. 641–658, 2000. https://doi.org/10.1023/A:1010167626551

[4] Muktham, R., Ball, A. S., Bhargava, S. K., Bankupalli, S. "Study of thermal behavior of deoiled karanja seed cake biomass: thermogravimetric analysis and pyrolysis kinetics", Energy Science & Engineering, 4(1), pp. 86–95, 2016. https://doi.org/10.1002/ese3.109

[5] Ponnam, V., Ghodke, P., Tondepu, S., Mandapati, R. "Thermal behaviour kinetic modeling of capsicum annuum waste biomass using an iso-conversion method", Journal of Thermal Engineering, 7(2), pp. 18–29, 2021. https://doi.org/10.18186/thermal.865555

[6] Sangeetha, R., Diea, Y. K. T., Chaitra, C., Malvi, P. G., Shinomol, G. K. "The amazing bamboo: a review on its medicinal and pharmacological potential", Indian Journal of Nutrition, 2(1), pp. 1–7, 2015.

[7] Silva, L. H. P., Tamashiro, J. R., Guedes de Paiva, F. F., Fernando dos Santos, L., Teixeira, S. R., Kinoshita, A., Antunes, P. A. "Bamboo leaf ash for use as mineral addition with Portland cement", Journal of Building Engineering, 42, 102769, 2021. https://doi.org/10.1016/j.jobe.2021.102769

[8] Mondal, D. K., Nandi, B. K., Purkait, M. K. "Removal of mercury (II) from aqueous solution using bamboo leaf powder: Equilibrium, thermodynamic and kinetic studies", Journal of Environmental Chemical Engineering, 1(4), pp. 891–898, 2013. https://doi.org/10.1016/j.jece.2013.07.034

[9] Kuntari, K., Fajarwati, F. I. "Utilization of bamboo leaves wastes for methylene blue dye adsorption", AIP Conference Proceedings, 2026(1), 020062, 2018. https://doi.org/10.1063/1.5065022

[10] Okeola, A. A., Abuodha, S. O., Mwero, J. "Experimental Investigation of the Physical and Mechanical Properties of Sisal Fiber-Reinforced Concrete", Fibers, 6(3), 53, 2018. https://doi.org/10.3390/fib6030053

[11] Lilargem Rocha, D., Tambara Júnior, L. U. D., Marvila, M. T., Pereira, E. C., Souza, D., de Azevedo, A. R. G. "A Review of the Use of Natural Fibers in Cement Composites: Concepts, Applications and Brazilian History", Polymers, 14(10), 2043, 2022. https://doi.org/10.3390/polym14102043

[12] Thyavihalli Girijappa, Y. G., Mavinkere Rangappa, S., Parameswaranpillai, J., Siengchin, S. "Natural Fibers as Sustainable and Renewable Resource for Development of Eco-Friendly Composites: A Comprehensive review", Frontiers in Materials, 6, 226, 2019. https://doi.org/10.3389/fmats.2019.00226

[13] Richter, F., Rein, G. "The Role of Heat Transfer Limitations in Polymer Pyrolysis at the Microscale", Frontiers in Mechanical Engineering, 4, 18, 2018. https://doi.org/10.3389/fmech.2018.00018

[14] Chong, C. T., Mong, G. R., Ng, J.-H., Chong, W. W. F., Ani, F. N., Lam, S. S., Ong, H. C. "Pyrolysis characteristics and kinetic studies of horse manure using thermogravimetric analysis", Energy Conversion and Management, 180, pp. 1260–1267, 2019. https://doi.org/10.1016/j.enconman.2018.11.071

[15] Kumar, M., Sabbarwal, S., Mishra, P. K., Upadhyay, S. N. "Thermal degradation kinetics of sugarcane leaves (*Saccharum officinarum* L) using thermo-gravimetric and differential scanning calorimetric studies", Bioresource Technology, 279, pp. 262–270, 2019. https://doi.org/10.1016/j.biortech.2019.01.137

[16] Liu, H., Wang, C., Zhao, W., Yang, S., Hou, X. "Pyrolysis characteristics and kinetic modeling of Artemisia apiacea by thermogravimetric analysis", Journal of Thermal Analysis and Calorimetry, 131(2), pp. 1783–1792, 2018. https://doi.org/10.1007/s10973-017-6599-3

[17] Kaur, R., Gera, P., Jha, M. K., Bhaskar, T. "Pyrolysis kinetics and thermodynamic parameters of castor (*Ricinus communis*) residue using thermogravimetric analysis", Bioresource Technology, 250, pp. 422–428, 2018. https://doi.org/10.1016/j.biortech.2017.11.077